Progress In Electromagnetics Research M, Vol. 19, 183–195, 2011

FOCUSING GROUND PENETRATING RADAR IMAGES WITH VERTICAL OFFSET FILTERING

A. Benter*, W. Moore, and M. Antolovich

School of Computing and Mathematics, Charles Sturt University, Panorama Avenue, Bathurst 2795, Australia

Abstract—Existing focusing techniques for Ground Penetrating Radar (GPR) rely on migration of 2D or 3D images to remove clutter originating from objects laterally offset from the antenna. In applications requiring real-time focusing, a method operating on 1D trace data is required. This paper presents a new algorithm for focusing GPR images, the Vertical Offset Filter (VOF), using simulated and real GPR data.

1. INTRODUCTION

GPR provides a mechanism to detect reflected signals from subsurface objects and changes in the electromagnetic characteristics of the ground material. Typically, the subsurface environment under study requires the GPR antenna to be moved horizontally across the surface of the ground. At individual locations, a signal 'trace' of reflections (an A-scan) from features illuminated by the GPR antenna is recorded. Multiple traces are compiled to form a B-scan. B-scans can then be processed to form a 3-dimensional profile of the underground features (referred to as a C-scan).

GPR has been used for archaeological discovery [1], non-destructive testing of engineering structures [2, 3], examination of ground soil characteristics and voids [4], and detection of buried land mines [5]. These activities utilise the GPR antenna in the typical way by moving parallel to the ground surface, obtaining signals with a common ground offset.

A significant limitation of GPR in such an application is clutter. Reference [6] suggests that the primary goal of signal processing is to

Received 2 June 2011, Accepted 23 July 2011, Scheduled 31 July 2011

* Corresponding author: Allen Benter (abenter@csu.edu.au).

remove or reduce clutter from the GPR return signal. Due to the broad beam width of the GPR signal, clutter is the result of reflections from objects within the beam other than the target, including those offset from the position of the antenna, and may include objects directly beneath the antenna.

A major source of clutter is the reflection from the surface. In order to reduce this, the antenna is, in a typical application, closely coupled to the surface during acquisition to direct the signal into the ground. Close coupling also has the effect of focusing the signal [7]. While it is normally desirable to achieve a close coupling between antenna and the ground surface, in some situations this is not possible.

One application of GPR that is of particular interest to the mining industry and the authors is to identify the presence of large rocks in the rubble formation at the draw point of an underground mine. After blasting, the fractured ore is collected from the draw point and taken to the primary crusher. Fragments larger than the primary crusher can accommodate may be hidden from view beneath the surface at the draw point. Due to the very course nature of the ore presentation, it is not possible, in a production setting, to achieve a close coupling with the ore surface. Whilst elevating the antenna results in a larger initial reflection from the surface, it also has the effect of reducing the signal response from subsurface objects that are horizontally offset from the antenna [7].

This paper presents a novel method to focus GPR signals. The following sections will describe a new algorithm for removing features within the beam of the GPR system, but not directly beneath the antenna. Section 2 will detail the VOF focusing algorithm; Section 3 will show simulated results using MatGPR [8]. Section 4 will then look at the application of the algorithm to real GPR data under controlled conditions, followed by Section 5 showing further work in the application and development of this algorithm.

2. FILTERING ALGORITHMS

Most GPR systems use a broad beam antenna, detecting reflected energy from subsurface structures. Given the broad beam width, objects illuminated by the antenna pulse, including those offset horizontally from the antenna position, contribute to the radar signal. Hence, the interpretation of a single time response is limited to the range of an object [9]. No information regarding horizontal offset can be inferred from the signal.

As the antenna is moved across the surface, the range to the illuminated object also changes — firstly decreasing as the antenna

approaches until the shortest range is recorded when the antenna is directly above the object, then increasing as the antenna moves past and beyond the object. This change is depicted in B-scans as a hyperbola.

This hyperbole structure is an unfocused depiction of the scatterer [10] which is removed using various migration processes. These are generally derived from seismic imaging research, and include the maximum convexity migration algorithm. The maximum convexity migration algorithm works by comparing each and every sample point across the entire B-scan. Each sample point that falls on a curve of maximum convexity is considered to be a reflection from the same point, and can be removed [11]. Thus, knowing the propagation speed of the signal through the media, or assuming a constant speed as required by maximum convexity migration, we can remove the hyperbole. In the case where we do not know the propagation speed, or the speed is variable, we need another method.

Recording signal returns from objects within the field of view, but offset from the antenna clutters the signal return from objects directly beneath the antenna. The hyperbole structure also contribute to the clutter in an image by interfering with the signal return in adjacent traces. Removing surface clutter from images using time gating has the undesired effect of removing the reflections from shallow objects. Averaging also works to remove coherent clutter, but is ineffective in inhomogeneous material. Removal of incoherent clutter is based on a statistical knowledge of the background material, or the target. In inhomogeneous material, the properties will vary. Using *a priori* knowledge of the target reflection [12] or shape [13] to build a reference signal is less useful when the target shape is unknown.

Figure 1(a) shows a simulated B-scan of two objects with a relative permittivity value of 3.5 ($\epsilon_r = 3.5$) located in free space (ϵ_0), and Figure 1(b) shows a typical A-scan trace along the dotted vertical line in Figure 1(a) (at about 0.5 m along the scan axis). The change in signal amplitude at 2.67 ns identifies the top of the box. Another signal change at 5.27 ns identifies the bottom of the box.

In a simulated GPR scan, we hold *a priori* knowledge of the position of the object which allows us to confirm the vertical position of the object in the A-scan. In a measured GPR scan, we do not possess this knowledge, therefore we cannot be certain the two peaks were return signals from the same object, or in fact, may indicate a separate object within the field of view of the antenna.

In material with a known constant velocity, the depth from emitter to reflector is given by $z = vt/2$, where t is the measured time to the reflector and v is the velocity of the signal through the material. The

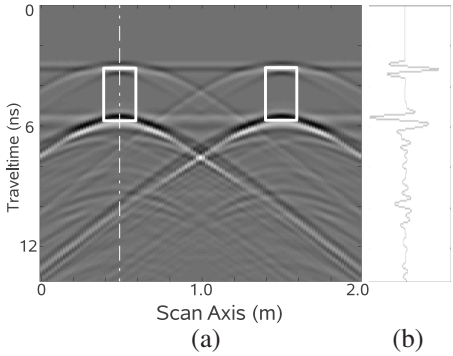

Figure 1. Synthetic scan of two objects ($\epsilon_r = 3.5$) located in free space ($v = 0.29979\,\mathrm{m/ns}$). (a) B-Scan, (b) A-scan.

typical hyperbolic pattern of a point reflector in motion across a B-scan is given by equation (from reference [6])

$$z_i = \sqrt{(x_i - x_0)^2 + z_0^2} \tag{1}$$

Ideally, we would have a pencil-thin beam to illuminate only those objects directly beneath the antenna. Given the wide-beam of the radar signal, if we could determine where in the radar beam the signal return originated, we could filter signal returns from laterally offset objects. With a single radar measure, we cannot determine the lateral offset position, and so Equation (1) remains as a range equation. However, if we record a trace, and move the antenna some distance h along the signal propagation path (that is, away from the ground) we can expect objects that are located directly beneath the antenna to also move h in the trace, such that

$$z_i = (z_0 + h) \tag{2}$$

Equation (1) thus becomes

$$z_i = \sqrt{(x_i - x_0)^2 + (z_0 + h)^2} \tag{3}$$

such that if $z_i \neq z_0 + h$ then the point reflector is not located on the signal propagation path and z_i can be clipped from the trace. Thus, the trace data only identifies objects directly beneath the antenna. Whilst not determining the lateral offset to objects, we are excluding those objects clearly not located directly beneath the antenna. We propose a new method called the Vertical Offset Filter, as shown below:

foreach *A-Scan* x_i **do**
  foreach *Offset A-Scan* $x_{i,k}$ **do**
    forall *Sample Values* $z_{i,k}$ **do**
      if $z_{i,k}$ *is a signal peak* **then**
        $s_{i,k} = 1$;
      else
        $s_{i,k} = 0$;
      end
    end
  end
  Align k scans by vertical offset h;
  $z_i = \sum_{k=1}^{m} s_{i,k}$;
  if $z_i == m$ **then**
    $z_i = 1$ //keep common signal peak;
  else
    $z_i = 0$ //discard signal peak;
  end
end

Algorithm 1: The Vertical Offset Filter (VOF) algorithm.

The VOF improves the maximum convexity migration method by working only on individual A-scans, rather than the entire B-scan data. This reduces the computational cost to a 1-D processing method, while also allowing construction of B-scans or C-scans. The novel method employed to achieve this improvement is the vertical offset obtained from the physical motion of the radar antenna, thus allowing the filter to remove all signal movements not matching the physical movement. This method does not require *a priori* knowledge of the propagation speed, or the location of the target, in order to remove clutter. The algorithm exploits the fact that the wave shape flattens as the antenna is elevated, as reported in [7].

The algorithm requires a data set comprised of multiple A-scans collected at the same surface position x_0. Each A-scan is offset in the vertical direction, that is, along the line of signal propagation by some distance h.

For each A-scan in the data set, the signal is adjusted for the vertical offset distance h. Signal peaks in each A-scan are identified as local *maxima* and used to create a binary mask. Following a summation over all the binary masks, those signal peaks that do not occur at the same time in each A-scan are excluded. The resulting mask is a binary mask of common signal peaks across each of the subject A-scans in the set of A-scans recorded at a distinct position.

Focusing GPR data using standard migration techniques requires

the capture of B-scans or C-scans prior to migration processing. The VOF algorithm operates on A-scans and, as long as the antenna is moved perpendicular to the ground, could operate in real-time to remove these artifacts.

Figure 2 shows three individual traces recorded at the same surface position. Each trace has been aligned in the vertical plane to allow for the vertical offset at the time of recording. The alignment offset is calculated for each A-scan using corresponding peaks in the data set.

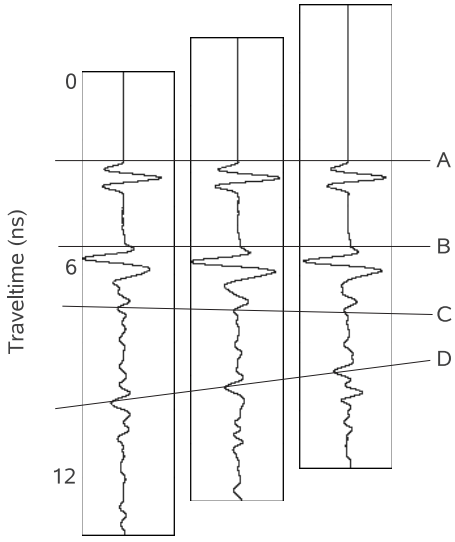

Figure 2. Individual traces recorded at the same location with a vertical offset highlighting the non-stationary data.

The set of traces is then examined, and positive peaks that occur in each trace are retained, while those that do not occur at the same relative time in each trace are discarded. For example, in Figure 2, common peaks are identified at positions **A** and **B**, as indicated by the horizontal lines. Non-stationary signal peaks are evidenced by identifying movement within the time domain, shown by the slightly sloped line **C** and more pronounced slope of line **D** indicating a decline and an incline, respectively. By removing these non-stationary signals we are left with only the stationary signals, which corresponds to those features located immediately below the antenna.

3. SYNTHETIC RESULTS

To demonstrate the algorithm, a GPR scan was synthesised using MatGPR [8]. The environment described was a 2.0 m wide by 1.0 m deep scan area of free space ($v = 0.29979$ m/ns). The space contained two objects of dimension 0.2 m × 0.2 m located at a depth of 0.4 m with a relative permittivity value $\epsilon_r = 3.5$. Synthetic scans were produced using a finite-difference time domain (FDTD) 2D method simulating a 1200 MHz antenna.

In total, three synthetic scans were simulated over the same surface path, each with a different vertical offset. The 0.00 m offset represents the initial position of the antenna. The 0.15 m and 0.30 m vertical offsets were chosen arbitrarily.

Figure 1 shows the raw GPR data obtained and presented as (a) a B-scan and (b) an A-scan through the centre of the left-hand object (represented in the B-scan as a dotted line). Although a very simple simulation, the images show the hyperbole from the top and bottom of the objects. It is also apparent that the hyperbola of the right-hand object also appears beneath the left-hand object. Hence, the A-scan through the left-hand object contains signal response from the right-hand object.

After the operation of the VOF algorithm, the image in Figure 3, titled 'VOF', is obtained. As can be seen, the hyperbole structures have been removed, and the image consists essentially of the top and bottom of the objects. For comparison purposes, Figure 3 shows a section of the raw B-scan ('RAW') showing only the left object, and the same section after application of the Vertical Offset Filter ('VOF').

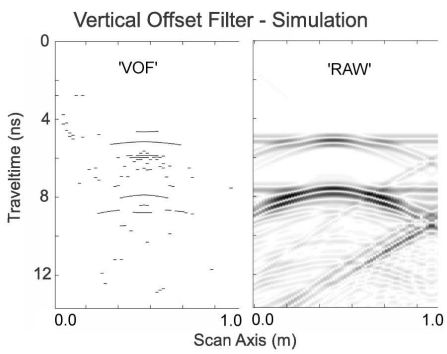

Figure 3. Raw synthetic data (RAW) and after the Vertical Offset Filter applied (VOF).

4. REAL RESULTS

The synthetic experiments were repeated using a 2 GHz Siropulse GPR system from CSIRO (Aust). The test environment was assembled by placing the sample on an 3 mm aluminium plate, with the antenna suspended from a timber rail directly above the sample. The antenna was then run along the rail, recording a B-scan over the sample.

In the first set of experiments, the sample was a solid piece of wood of dimensions 0.17 m × 0.17 m × 0.10 m (LxDxW) supported on a dowel base to a height of 0.49 m above the metal plate (see Figure 4). Figure 5(a) shows the raw data obtained from the GPR system. The image shows a dominant reflection from the metal plate and loud antenna ringing in the early time interval. There was also some dipping features in the traces between 0–0.5 m and 1.2–2.0 m caused by the supports of the antenna rail. The wood block is not immediately obvious in the unfiltered image, however the top can be seen at about 2.5 ns.

Three scans were recorded, with the antenna lifted vertically 100 mm between the scans, thus creating an offset in the vertical direction. Before the VOF could be applied to the data set, the three scans needed to be aligned. The three data sets were manually aligned by identifying the midpoint between the first arrival of the leading edge of the sample, and the last arrival of the trailing edge of the sample. The data sets were trimmed of traces to a common length, and zero-padding was applied to the offset data to ensure the scans had a common depth. The resulting data sets were three B-scans of the same depth and width, with data vertically offset by an amount equal to the vertical lift of the antenna.

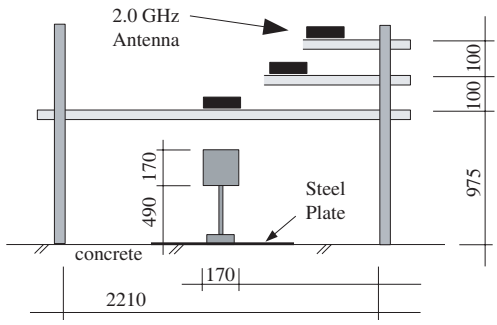

Figure 4. Experimental setup to capture VOF data over a wood block similar to the simulated scans.

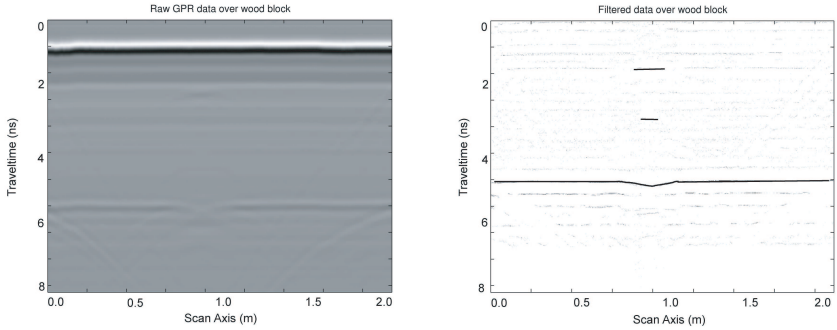

(a) Raw data (b) VOF filtered data

Figure 5. Real GPR scans over wood block.

After filtering the images with the VOF, Figure 5(b) was obtained. The steel sheeting on the floor was immediately apparent at about 5 ns. The top of the wood block was visible at about 1.5 ns which corresponds to the shifted raw data. The top of the block was recorded across 158 samples. Based on the horizontal spacing of 1.15 mm/trace, the top of the wood block was calculated to be 0.18m, closely matching the actual dimensions. The bottom of the wood block is apparent at about 3 ns. The image also presents the dipping floor under the object representing the reduced velocity of the signal through the higher relative permittivity of the wood block.

Further experiments were conducted on complex samples of rock fragments. Rock samples were obtained and manually sifted to uniform fragment sizes of < 25 mm, 25–50 mm and 50–100 mm. These were randomly placed in separate plastic boxes of dimensions $0.5\,\text{m} \times 0.2\,\text{m} \times 0.4\,\text{m}$ (LxDxW) and placed on an aluminium plate (see Figure 6). Figure 7(a) shows the raw data from the GPR unit. In this image it can be seen that the floor presented, as in the previous experiment with the wood block, as a continuous and solid reflection generally at a constant time. The rock fragments are observed as a turbulent area in the centre of the image.

Faint artifacts are present from about 2 ns until the concrete floor in early and late traces which are reflections from the supporting structure for the antenna. There are also considerable reflections appearing below the floor, however these are multipath/late arrival reflections from the sides of the structure and the beam supporting the antenna. These artifacts are considered unwanted reflections cluttering the image.

Once again the images were manually aligned, in a similar method

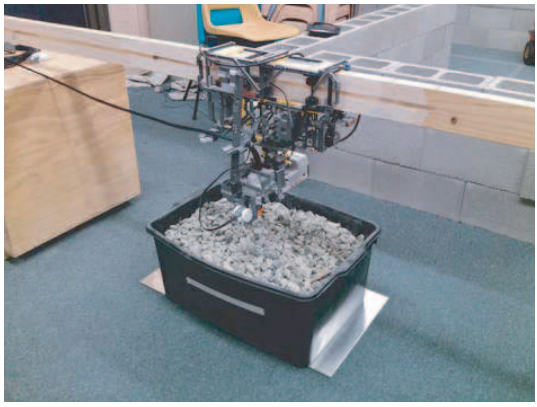

Figure 6. Experimental setup to capture VOF data over rock samples.

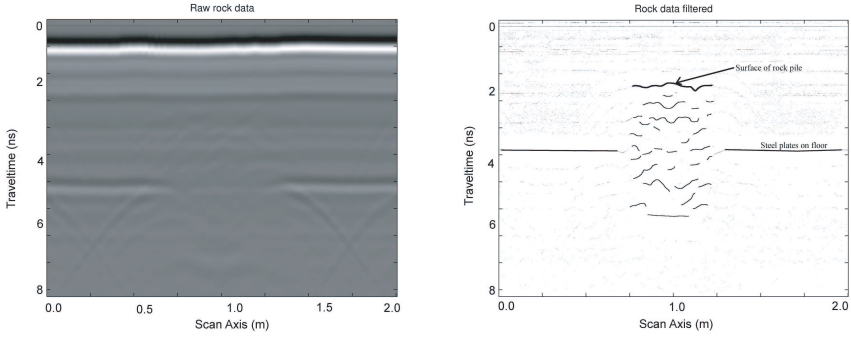

(a) Raw data (b) VOF ltered data

Figure 7. Scan over plastic container of rock fragments 25 mm to 50 mm.

to that above, before the VOF was applied to the combined data. The Images were aligned using the floor as a common vertical component to determine the actual vertical offset. The horizontally alignment used the leading edge of the container as a common feature in the three b-scans.

After application of the VOF over the images, Figure 7(b) was obtained, which showed the surface profile of the rock fragments, the steel floor, and significant reflections beneath the surface. The floor is shown at about 6 ns due to the effect of the change in velocity of the signal by the increased permittivity of the rocks. The side reflections and multipath/late arrival reflections have all been removed.

The image has been augmented to assist interpretation by tracing the significant reflections from the surface of the rocks, within the container.

The footprint of the antenna beam was approximately 1 m in the x and y directions at the elevations used. The surface profile depicted in the images corresponded with the surface profile of the rock fragments providing a much finer resolution than the footprint would suggest possible.

5. DISCUSSION

It has been shown in Figure 3 that the VOF improves the resolution of the simulated data, removing clutter from the original. The operation is also very fast over each A-scan data set, and allows construction of B-scans from the filtered data. The algorithm has also been implemented on real GPR data (Figures 5(b) and 7(b)) and showed similar clutter removal in the filtered B-scan. Further experiments are required to determine the resolution of the data filtered using VOF, and to refine the operation to reduce signal decimation.

There is an additional cost associated with using the authors algorithm in the acquisition of the data set. The VOF requires at least 2 identical A-scans with a vertical shift occurring between the two scans. This additional acquisition time may be a problem in certain applications. In the particular application under study (see Section 1) this additional cost can be reduced by using a horizontal array of antennas and the motion of the image acquisition vehicle. As the vehicle approaches the draw point, the antennas will be offset in relation to the draw point — equivalent to the vertical offset in Figures 2, 3, 4 and 5. Each set of traces can then be processed individually, with an adjustment for the offset distance. The processed trace data can then be compiled to create a B-scan for further image analysis.

The real data sets presented in this paper were manually aligned before applying the VOF algorithm. In the application presented above, data would normally be collected as A-scans. The vertical alignment offset can be easily calculated from either the first arrival reflection, or using additional sensors, such as a laser sensor. As long as the vehicle is approaching perpendicular to the sample, the data is likely to be horizontally aligned. In other applications, the setup and acquisition of A-scans would need to consider the alignment in the vertical and horizontal planes.

6. CONCLUSION

This paper has presented a novel method to focus real and simulated GPR data. The method focuses the GPR image through the removal of clutter which also removes the hyperbola structure commonly associated with GPR data. The resulting image can assist in determining the size and location of objects directly beneath the antenna. The algorithm is also efficient in processing time, and in certain circumstances can operate in real time on the removal of these artifacts.

Further analysis of the data is required to demonstrate the resolution achievable under operation of the filter, and the correspondence of interior reflections to objects within the target structure. Further work is also proposed in automating the algorithm to determine the offset in complex environments.

ACKNOWLEDGMENT

This research is being conducted as part of a research program funded by Newcrest Mining Ltd. The authors would like to thank the reviewers for their constructive comments which have improved this paper.

REFERENCES

1. Conyers, L. B. and T. Osburn, "GPR mapping to test anthropological hypotheses: A study from comb wash., utah, american southwest," *11th International Conference on Ground Penetrating Radar*, 2006.
2. Leucci, G., S. Negri, and M. T. Carrozzo, "Ground penentrating radar (GPR): An application for evaluating the state of maintenance of the building coating," *Annals of Geophysics*, Vol. 46, No. 3, 481–489, 2003.
3. Willett, D., K. Mahboub, and B. Rister, "Accuracy of ground-penetrating radar for pavement-layer thickness analysis," *Journal of Transportation Engineering*, Vol. 132, No. 1, 96–103, 2006.
4. Chen, Y. L. and J. J. Chow, "Ground penetrating radar signal processing improves mapping accuracy of underground voids and seawater table: An application in deteriorating coastal structure, nanfango port, taiwan," *Environmental Geology*, Vol. 53, 445–455, 2007.
5. Rappaport, C., M. El-Shenawee, and H. Zhan, "Suppressing GPR clutter from randomly rough ground surfaces to enhance

nonmetallic mine detection," *Subsurface Sensing Technologies and Applications*, Vol. 4, No. 4, 311–326, 2003.

6. Daniels, D., *Geound-Penetrating Radar* , IET, New York, 2004.
7. Bloemenkamp, R. and E. Slob, "The effect of the elevation of GPR antennas on data quality," *2nd International Workshop on Advanced GPR*, 2003.
8. Tzanis, A., "Matgpr: A freeware matlab package for the analysis of common-offset GPR data," *Geophysical Research Abstracts*, Vol. 8, No. 09448, 2006.
9. Plumb, R. G. and C. Leuschen, "A class of migration algorithms for ground penetrating radar data," *IGARSS99*, 2519–2521, 1999.
10. Ozdemir, C., S. Demirci, and E. Yigit, "Practical algorithms to focus B-scan GPR images: Theory and application to real data," *Progress In Electromagnetic Research B*, Vol. 6, 109–122, 2008.
11. Upadhyay, S., *Seismic Reflection Processing*, Springer, 2007.
12. Van Der Merwe, A. and I. J. Gupta, "A novel signal processing technique for clutter reduction in GPR measurements of small, shallow land mines," *GeoRS*, Vol. 38, No. 6, 2627–2638, 2000.
13. Kovalenko, V., A. G. Yaravoy, and L. P. Ligthart, "A novel clutter suppression algorithm for landmine detection with GPR," *IEEE Trans. on Geoscience and Remote Sensing*, Vol. 45, No. 11, 3740–3751, 2007.